

Single-Cycle Optical Control of Beam Electrons

Yuya Morimoto^{1,*} and Peter Baum^{1,2,†}¹Ludwig-Maximilians-Universität München, Am Coulombwall 1, 85748 Garching, Germany²University of Konstanz, Universitätsstraße 10, 78457 Konstanz, Germany

(Received 2 July 2020; accepted 25 September 2020; published 3 November 2020)

We report the single-cycle optical control of a freely propagating electron beam with an isolated cycle of midinfrared light. In particular, we produce and characterize a modulated electron current with peak-cycle-specific subfemtosecond structure in time. The direct effects of the carrier-envelope phase, amplitude, and dispersion of the optical waveform on the temporal composition, pulse durations, and chirp of the free-space electron wave function demonstrate the subcycle nature of our control. These results and concept may create novel opportunities in free-electron lasers, laser-driven particle accelerators, ultrafast electron microscopy, and wherever else high-energy electrons are needed with the temporal structure of single-cycle light.

DOI: 10.1103/PhysRevLett.125.193202

Modern attosecond science aims at the exploration of ultrafast charge carrier dynamics in complex materials by investigating the time-dependent responses of bound electrons to a single cycle of optical excitation. The electric field as a driving force can, for example, produce macroscopic electric currents [1,2] or spin waves [3] as a consequence of electronic motion on atomic dimensions. While such light-cycle control of low-energy electrons is ideal for ultrafast electronic operations or for the generation of intense attosecond light pulses, a single-cycle control of the temporal, spatial, and energetic structure of high-energy electron beams would be crucial for laser-driven particle accelerators [4,5], ultrafast electron imaging [6,7], electron-based quantum information technology [8], or attosecond science with free-electron lasers [9,10]. However, so far only radio frequency fields [11–13], terahertz radiation [14–17], or optical multicycle pulses [4,5,18–21] have been employed for the acceleration, compression, or metrology of free-space electron pulses on timescales of tens of femtoseconds [12–14,16,17] or in the form of multipulse sequences [4,5,18–21]. Although pioneering electron acceleration experiments were reported with few-cycle laser pulses [22–24], it remains to be established whether and how an isolated optical field cycle can control the temporal shape of free-space electrons at keV–MeV energies with attosecond precision, in order to merge the unprecedented power and brightness of high-energy electron beams with the temporal structure provided by single-cycle laser light.

The concept and sketch of our experiment are shown in Figs. 1 and 2(a), respectively. A femtosecond ytterbium potassium gadolinium tungstate (Yb:KGW) laser (magenta) is used for generating a beam of 70-keV electron pulses (blue) and for pumping a midinfrared optical parametric amplifier [25] for single-cycle waveform generation.

Briefly, near-infrared (NIR) pulses (orange) from the non-collinear optical parametric amplifier (NOPA) are mixed with fundamental pulses from the Yb:KGW laser (magenta) in a LiGaS₂ crystal for difference-frequency generation. Passive phase locking produces midinfrared pulses with a stable carrier-envelope phase. The spectrum [see Fig. 2(b)] spans from 26 THz (11.5 μm) to 62 THz (4.8 μm) at –20 dB level, exceeding one optical octave. The temporal waveform is characterized by electro-optical sampling and shown in Fig. 2(c). The main field cycle at $t \approx 0$ fs is 1.8 times stronger than the adjacent positive peaks at $t \approx \pm 23$ fs and the pulse shape therefore allows a subcycle control of the electron beam. A split and displaced parabolic mirror (yellow) focuses two such pulses onto ultrathin membranes (green) for temporal modulation of the electron wave packet (blue) and its subsequent streaking characterization. The amplitude and the carrier-envelope

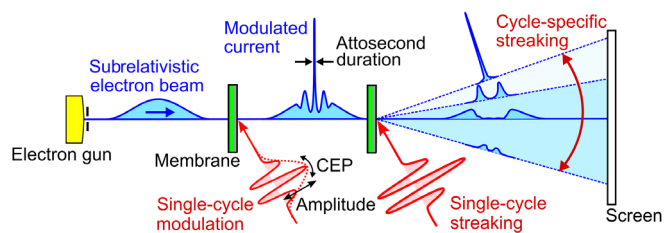


FIG. 1. Concept of single-cycle electron-beam control. An electron beam (blue) is modulated by a single field cycle (red) of a phase-controlled waveform when passing through a free-standing metallic membrane (green). The temporally modulated electron current is directly characterized by real-space streaking induced by a second single-cycle field (red). The streaking by the isolated peak half-cycle spatially isolates a single attosecond peak of the modulated current.

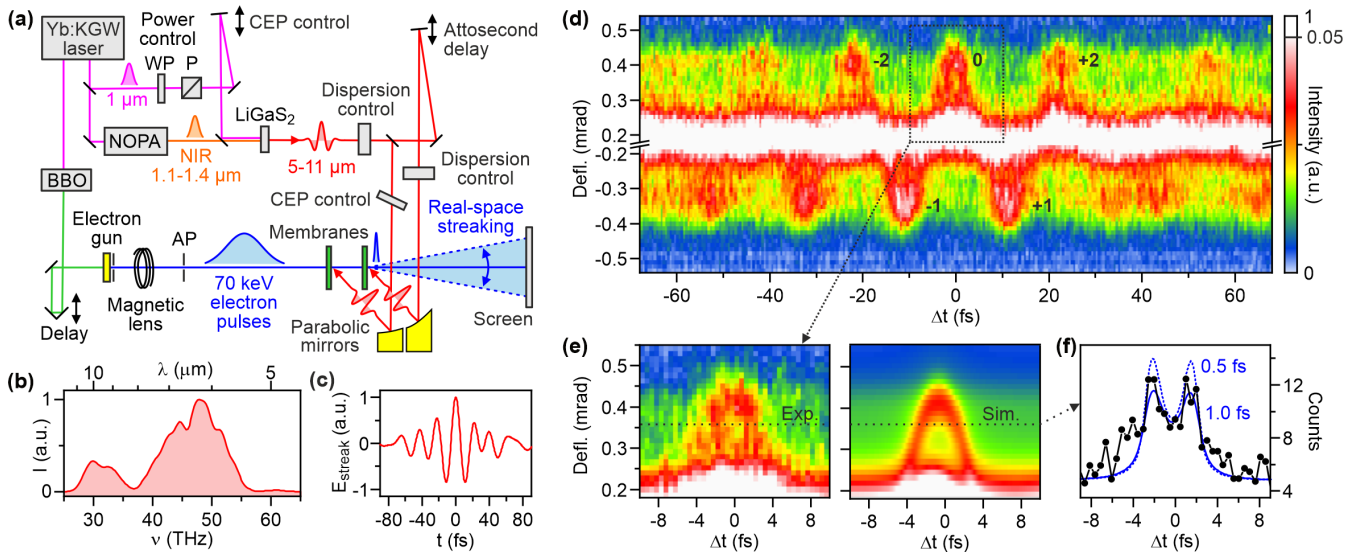


FIG. 2. Single-cycle control of subrelativistic beam electrons. (a) Experiment. A collimated 70-keV electron beam of 100 μm diameter (2500 electrons/s) is temporally modulated and analyzed by a single optical cycle of a midinfrared field (red). WP, wave plate; P, polarizer; AP, aperture. (b) Spectrum of the midinfrared pulses. (c) Electric field waveform of the midinfrared pulses. (d) Streaking signal of the temporally modulated electron pulses as a function of the modulation-streaking delay Δt . Peak 0: electron’s peak current streaked by the isolated positive cycle. Peak ± 1 : peak current streaked by the negative field peaks. Peak ± 2 : side peak current streaked by the isolated cycle. (e) Streaking signal of the central feature (left) in comparison to a simulation (right) for an electron pulse duration of 1.0 fs (full width at half maximum). (f) Slice of the streaking pattern at an angle of 0.37 mrad. The observations (black circles) range between a simulation with an electron pulse duration of 1.0 fs (blue solid curve) and 0.5 fs (blue dotted curve).

phase (CEP) of the two midinfrared pulses are adjusted independently [see Fig. 2(a)].

In order to control the electron beam by a single cycle of light (red), we invoke electron-transparent metallic membranes with an extremely broad bandwidth as the modulation elements for photon-electron energy exchange [26,27]. Freestanding silicon nitride membranes are coated with ~ 10 nm of aluminum. Although this coating is >500 times thinner than the wavelength, we find that the membranes reflect our single-cycle midinfrared pulses efficiently over the full range of their octave-broad spectrum. The 70-keV electrons pass through the membrane within a time of <0.14 fs and are therefore injected into the optical electromagnetic field on the backside within sub-cycle time. This abrupt injection from a field-free region before the membrane into the optical field cycles on the backside causes a time-dependent electron energy modulation that follows the temporal integral of the optical waveform [26,28], an effect that closely resembles attosecond methodology using photoionization [29–31]. At the first membrane, the one for single-cycle temporal modulation, we apply an optical peak field strength of ~ 25 MV/m. Vacuum is a dispersive medium for our electrons and the cycle-induced energy modulation is therefore transformed by propagation into a modulation of current density in time [19]. We characterize the final electron pulse shape at a distance of ~ 12 mm at a second metal membrane under illumination of a stronger single-cycle field at ~ 200 MV/m that produces a field-driven

sideways electron deflection as a function of time [14]. This real-space streaking by a single-cycle field isolates the compressed electron pulses in transverse momentum space with subfemtosecond precision (see Fig. 1) and therefore provides a direct metrology of the effects of the first interaction’s single-cycle control in time. The second membrane is placed in parallel to the first membrane for achieving attosecond resolution free of laser-electron velocity mismatch effects [28,32].

Figure 2(d) shows the observed streaking pattern on the screen, plotted as a function of the delay Δt between the control field and the streaking field. The largest streaking angle is more than 0.4 mrad, corresponding to the absorption or emission of more than 900 photons at 6.9 μm central wavelength. The highest streaking speed around $\Delta t \approx \pm 11$ fs is ± 0.1 mrad/fs, enabling attosecond time resolution [19,28]. There are pronounced streaking oscillations of sideways deflection as a function of delay, but unlike in previous cases with multicycle fields [19] we see here a streaking signal that does not repeat itself before or after one optical cycle of delay. In other words, the streaking peak shapes around $\Delta t \approx 0$ fs (peak 0; dotted rectangle) and around $\Delta t \approx \pm 23$ fs (peaks +2 and –2) differ substantially in magnitude and shape. These observations suggest the presence of one exceptional peak of electron density with subcycle duration within the pattern of compressed electron density in our beam.

The left panel of Fig. 2(e) shows a magnified view of the large-angle streaking signal around $\Delta t \approx 0$ fs [see

dotted rectangle in Fig. 2(d)]. The measured streaking intensity shows a broad maximum at the turning point around ~ 0.42 mrad, a hole with two separate borders in time at ~ 0.35 mrad (dotted line), and a temporally washed-out pattern at lower angles. Results of a numerical simulation (see Supplemental Material [33]) are depicted in the right panel of Fig. 2(e) for an electron pulse duration of 1.0 fs (full width at half maximum). A more detailed comparison between experiment and simulations is shown in Fig. 2(f), where we plot a cut through Fig. 2(e) at a deflection angle of 0.37 mrad. We see a high streaking intensity at $\Delta t \approx -2$ fs, followed by a minimum at $\Delta t \approx 0$ fs and again a maximum at $\Delta t \approx +2$ fs. This double peak in time with dip in the middle resembles almost the classical time-dependent deflection dynamics that would occur for electron pulses of negligible duration in time. Comparison of the measured data in Fig. 2(f) (black dots) to the results of the simulations (blue lines) indicates an electron pulse duration somewhere between 0.5 fs (dashed blue line) and 1.0 fs (solid blue line).

For a more profound characterization and for understanding the role of potential electron density peaks from adjacent compression cycles [see Fig. 3(a)], we consider the single-cycle nature of the streaking deflection at high angles [see Fig. 2(c)] and apply a numerical deconvolution and fitting procedure (see Supplemental Material [33]). Basically, streaking angles above 0.35 mrad can only originate from an isolated but finite range of time around $t = 0$ with few-femtosecond duration [see Fig. 2(c)]. A numerical consideration of the angular divergence of the electron beam, causing angular blurring in Fig. 2(e), provides a temporal instrument response function that we use for deconvolution (see Supplemental Material [33]). Figure 3(b) shows the resulting time-dependent electron current density as a function of the peak field strength of the central control cycle. A peaking electron density emerges at points in time where the electric field has positive peaks (dotted lines). There, we have a close-to-linear time-dependent acceleration; preceding electrons are decelerated and trailing electrons are accelerated. In contrast, there is no electron pulse compression at negative field peaks.

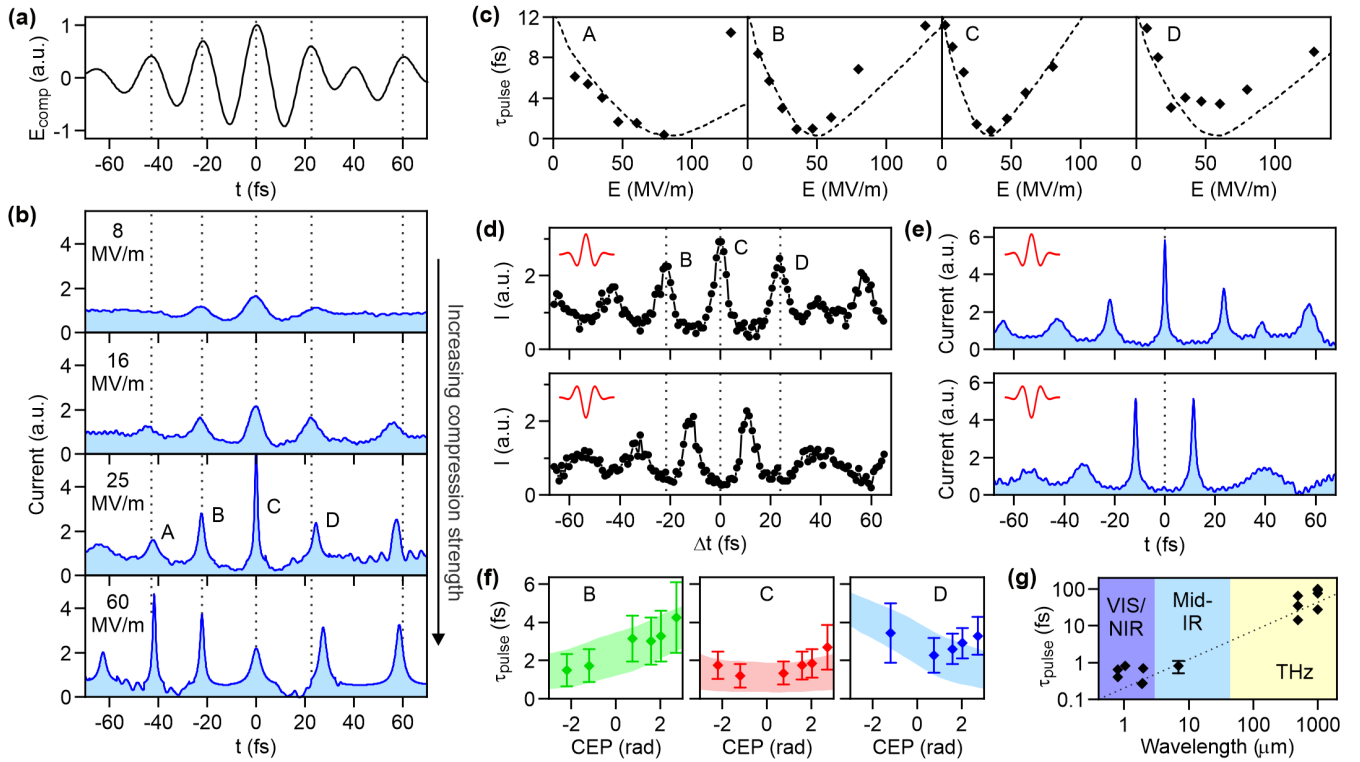


FIG. 3. Electron pulse formation and carrier-envelope phase effects. (a) Waveform of the modulation field. (b) Electron current density in dependence of an increasing modulation strength. (c) Electron pulse durations (black squares) for the four peaks A–D [see (b)] as a function of the field strength of the central cycle. The shortest full width at half maximum durations are (A) 0.6 ± 0.6 , (B) 0.9 ± 0.8 , (C) 0.8 ± 0.6 , and (D) 3.1 ± 1.8 fs. Dashed lines depict the result of quantum mechanical simulations. (d),(e) Carrier-envelope phase control. (d) Time-dependent intensity at highest streaking angle (>0.35 mrad) for a cosine field (upper) and for a minus-cosine field (lower). (e) Retrieved electron current density for the two control field shapes. The appearance of a single peak or double peaks is determined by the carrier-envelope phase. (f) Pulse durations (dots) of the peaks B–D as a function of the carrier-envelope phase. The transparent bands show the results of simulations with error margins. (g) Survey of the electron pulse durations so far obtained at different control wavelengths [4,5,14–21,41–44]. Single-cycle electron control is applicable to any wavelength for which an octave-broad modulation element can be designed (see Supplemental Material [33]).

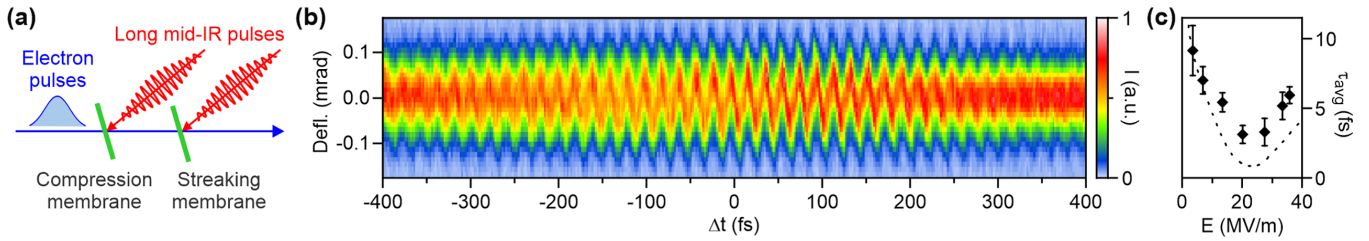


FIG. 4. Free-electron control with multicycle midinfrared fields. (a) Experimental scheme for multicycle midinfrared control. (b) Measured streaking data. The oscillation period, and therefore the temporal separation of the electron pulses, is ~ 21 fs. (c) Train-averaged electron pulse duration (dots) as a function of the compression field strength in comparison to the results of quantum mechanical simulations (dashed line).

Although the secondary positive field crests [peaks A, B, and D in Fig. 3(b)] can also create a bunched electron current, these cycles have lower field strengths and therefore produce distinguishable compression results. At ~ 25 MV/m, for example, peak C is well compressed, but all adjacent peaks are still long. A higher compression strength (lower panels) disperses the central peak toward longer duration and instead compresses the adjacent peaks A, B and D. Figure 3(c) shows the retrieved electron pulse durations (see Supplemental Material [33]) as a function of the compression strength; the dashed lines denote the results of quantum mechanical simulations [45]. We see that each of the optical cycles produces a minimum electron pulse duration at substantially different compression strength. Exceptional conditions are, for example, achieved at ~ 25 MV/m [third panel of Fig. 3(b)], where the central electron pulse C is almost isolated in time (assuming a full width at half maximum criterion), or again at ~ 80 MV/m, where we observe an overdispersion (depletion) of peaks B–D but emergence of an isolation of peak A (see Fig. S2 in the Supplemental Material [33]). In principle, any optical field cycle of the compression waveform that is unique with respect to the other field cycles can selectively optimize the compression of a single peak density of electrons in time, and subsequent single-cycle time-dependent sideways deflection [Fig. 2(d)] into a high-angle aperture isolates this pulse from the satellites and time-independent background (see Supplemental Material [33]) in a similar way to the attosecond lighthouse effect in high harmonic generation [46].

Further evidence for the single-cycle control of our electron beam can be obtained from a scan of the carrier-envelope phase ϕ_{CEP} of the compression waveform. Figures 3(d) and 3(e) show the raw high-angle streaking data at >0.35 mrad (black dots) and the retrieved electron density (blue) as a function of time for $\phi_{\text{CEP}} \approx 0$ (cosine waveform) and $\phi_{\text{CEP}} \approx \pm\pi$ (minus-cosine waveform); a continuous scan of ϕ_{CEP} is reported in the Supplemental Material [33]. With the cosine-shaped modulation field, we create an electron pulse structure with one exceptional peak [upper panels in Figs. 3(d) and 3(e)], but the minus-cosine-like modulation field produces two almost

equally high peaks [lower panels in Figs. 3(d) and 3(e)] that originate from the two previously negative field cycles at ± 11 fs [see Fig. 3(a)]. Figure 3(f) depicts the compressed electron pulse durations as a function of the carrier-envelope phase for the three peaks B–D in Fig. 3(d). The middle peak (C) has the shortest duration at $\phi_{\text{CEP}} = 0$ (cosine field), while peak B becomes shorter and peak D becomes longer when increasing ϕ_{CEP} . At $\phi_{\text{CEP}} \approx \pm\pi$ (minus-cosine field), peaks exchange places (see Supplemental Material [33]) and there emerges a double-peak structure [see lower panels in Figs. 3(d) and 3(e)]. We conclude that a simple change of the absolute direction of the control field produces electron current densities of substantially different shape in time.

It is also possible to produce a multipulse sequence of few-femtosecond electron pulses with longer midinfrared pulses (see Supplemental Material [33]) in which there are no single-cycle effects. At an optical pulse duration of ~ 800 fs [see Fig. 4(a)], the field cycles used for modulation and streaking have approximately equal field strength over the entire duration of the incoming electron pulses from the source (~ 500 fs). The observed delay-dependent streaking signal [Fig. 4(b)] therefore consists of tens of coherent oscillations over hundreds of femtoseconds, demonstrating the creation of multiple electron pulses with subcycle duration in synchrony to the optical cycles of the streaking field [19]. Carrier-envelope phase effects are indistinguishable from a delay in this experiment. Figure 4(c) shows the evaluated electron pulse duration as an average value over all the individual pulses in the sequence. There is an optimum shortness at ~ 25 MV/m, similar to the best field strength needed for the single-cycle control [compare Fig. 3(b)]. The shortest average pulse duration of 3.1 ± 0.7 fs (full width at half maximum) is a little longer than the best single-cycle results [≤ 1 fs; see Figs. 2(c) and 3(c)], because inelastic energy losses at the modulation membrane or differences of chirp of the involved laser and electron pulses may contribute to a varying duration of the different individual pulses in the burst. All such effects are irrelevant in case of the single-cycle control. Nevertheless, a cycle-locked few-femtosecond electron pulse train, in which the individual pulses are separated by tens of

femtoseconds instead of a few femtoseconds for NIR excitation [4,5,18–21], can be useful for waveform electron microscopy [19], electron acceleration [4,5], or quantum control of electron wave packets [47,48] in cases where isolated attosecond electron pulses are not necessarily required [19]. The fraction of useful electrons is approximately given by the ratio of the incoming electron pulse duration to the pulse duration of the laser field, in our experiments 2% with the single-cycle pulse (Figs. 2 and 3) and close to 50% with the long pulses in Fig. 4.

Taken together, the reported results demonstrate that the temporal shape of freely propagating high-energy electrons can be controlled and shaped by the field cycles of single-cycle light. Carrier-envelope phase effects demonstrate the dedicated influence of the central optical cycle and its absolute direction of the field for the temporal structure of compressed electron pulses. Two interactions with a dispersive section between them allow one to create compressed electron pulses that can be spatially isolated via sideways deflection. Attosecond science and metrology with electrons in isolated electromagnetic field cycles are therefore advanced from eV-level energies [1–3,49–54] into the subrelativistic and relativistic regime of the free-space electron beams. The only prerequisite of our approach is support of at least approximately one optical octave of bandwidth by the modulation element. Metal membranes [26,27], dielectrics or broadband absorbers [28], subwavelength resonators [14], or quasi-phase-matched devices [15,55] can fulfill such criterion with appropriate designs. For modulating higher-energy beams, key design criteria will be peak field resistance and efficient quasi-phase-matching.

The here demonstrated midinfrared control merges the two so far reported regimes of electron-beam control with either subpetahertz light [4,5,18–21] or with terahertz radiation [14–17]; see Fig. 3(g). In comparison to other proposals for isolated electron pulse generation out of a longer pulse, for example, by multicolor laser fields [14,21,56], we have a direct interferometric link to single-cycle pulses to be used for specimen excitation. The fraction of the temporally isolated electrons is given by the ratio of the initial pulse duration to the half-cycle period of the control field and ultimately limited by space charge to one or a few electrons per attosecond peak [14,21,56]. The resulting subcycle optical control of the energy, temporal shape, and space-time correlations of beam electrons with attosecond precision will, for example, enable the injection of isolated attosecond electron pulses into laser-driven particle accelerators [4,5], the attosecond-Angstrom imaging of complex material dynamics with electron microscopy or diffraction [19], the coherent control of quantum systems [57] and radiation processes [58], or the ultrafast modulation and tomography of free-electron quantum states [8,20,47] in energy and time. More generally, unifying the power and brightness of modern free-space

electron beams with the ultimate control of time by modern attosecond science via the concepts reported in this Letter may provide a general novel tool for exploring and controlling complex materials at unprecedented levels of flexibility, power, energy, and time.

We thank Bo-Han Chen and Christina Hofer for helpful discussions on midinfrared optics, Simon Stork and Jerzy Szerypo for membrane coating, Alexander Gliserin for help with measurement automation, and Ferenc Krausz for generous supply of laboratory infrastructure. Y.M. acknowledges general support from Peter Hommelhoff. This work was supported by the European Research Council (CoG No. 647771) and the Munich-Centre for Advanced Photonics.

*Corresponding author.

yuya.morimoto@fau.de

†Corresponding author.

peter.baum@uni-konstanz.de

‡Present address: Friedrich-Alexander-Universität Erlangen-Nürnberg, Staudtstraße 1, 91058 Erlangen, Germany.

- [1] A. Schiffrin, T. Paasch-Colberg, N. Karpowicz, V. Apalkov, D. Gerster, S. Mühlbrandt, M. Korbman, J. Reichert, M. Schultze, S. Holzner, J. V. Barth, R. Kienberger, R. Ernstorfer, V. S. Yakovlev, M. I. Stockman, and F. Krausz, *Nature (London)* **493**, 70 (2013).
- [2] T. Higuchi, C. Heide, K. Ullmann, H. B. Weber, and P. Hommelhoff, *Nature (London)* **550**, 224 (2017).
- [3] S. Schlauderer, C. Lange, S. Baierl, T. Ebnet, C. P. Schmid, D. C. Valovcin, A. K. Zvezdin, A. V. Kimel, R. V. Mikhaylovskiy, and R. Huber, *Nature (London)* **569**, 383 (2019).
- [4] D. S. Black, U. Niedermayer, Y. Miao, Z. Zhao, O. Solgaard, R. L. Byer, and K. J. Leedle, *Phys. Rev. Lett.* **123**, 264802 (2019).
- [5] N. Schönenberger, A. Mittelbach, P. Yousefi, J. McNeur, U. Niedermayer, and P. Hommelhoff, *Phys. Rev. Lett.* **123**, 264803 (2019).
- [6] A. H. Zewail, *Science* **328**, 187 (2010).
- [7] R. J. D. Miller, R. Ernstorfer, M. Harb, M. Gao, C. T. Hebeisen, H. Jean-Ruel, C. Lu, G. Moriena, and G. Sciaini, *Acta Crystallogr. Sect. A* **66**, 137 (2010).
- [8] K. E. Echternkamp, A. Feist, S. Schäfer, and C. Ropers, *Nat. Phys.* **12**, 1000 (2016).
- [9] A. A. Zholents and W. M. Fawley, *Phys. Rev. Lett.* **92**, 224801 (2004).
- [10] P. K. Maroju *et al.*, *Nature (London)* **578**, 386 (2020).
- [11] T. van Oudheusden, P. L. E. M. Pasmans, S. B. van der Geer, M. J. de Loos, M. J. van der Wiel, and O. J. Luiten, *Phys. Rev. Lett.* **105**, 264801 (2010).
- [12] A. Gliserin, M. Walbran, F. Krausz, and P. Baum, *Nat. Commun.* **6**, 8723 (2015).
- [13] J. Maxson, D. Cesar, G. Calmasini, A. Ody, P. Musumeci, and D. Alesini, *Phys. Rev. Lett.* **118**, 154802 (2017).
- [14] C. Kealhofer, W. Schneider, D. Ehberger, A. Ryabov, F. Krausz, and P. Baum, *Science* **352**, 429 (2016).

- [15] D. Zhang, A. Fallahi, M. Hemmer, X. Wu, M. Fakhari, Y. Hua, H. Cankaya, A.-L. Calendron, L. E. Zapata, N. H. Matlis, and F. X. Kärtner, *Nat. Photonics* **12**, 336 (2018).
- [16] L. Zhao *et al.*, *Phys. Rev. X* **8**, 021061 (2018).
- [17] D. Ehberger, K. J. Mohler, T. Vasileiadis, R. Ernstorfer, L. Waldecker, and P. Baum, *Phys. Rev. Applied* **11**, 024034 (2019).
- [18] C. M. S. Sears, E. Colby, R. Ischebeck, C. McGuinness, J. Nelson, R. Noble, R. H. Siemann, J. Spencer, D. Walz, T. Plettner, and R. L. Byer, *Phys. Rev. ST Accel. Beams* **11**, 061301 (2008).
- [19] Y. Morimoto and P. Baum, *Nat. Phys.* **14**, 252 (2018).
- [20] K. E. Priebe, C. Rathje, S. V. Yalunin, T. Hohage, A. Feist, S. Schäfer, and C. Ropers, *Nat. Photonics* **11**, 793 (2017).
- [21] M. Kozák, N. Schönenberger, and P. Hommelhoff, *Phys. Rev. Lett.* **120**, 103203 (2018).
- [22] K. Schmid, L. Veisz, F. Tavella, S. Benavides, R. Tautz, D. Herrmann, A. Buck, B. Hidding, A. Marcinkevicius, U. Schramm, M. Geissler, J. Meyer-ter-Vehn, D. Habs, and F. Krausz, *Phys. Rev. Lett.* **102**, 124801 (2009).
- [23] M. Kozák, M. Förster, J. McNeur, N. Schönenberger, K. Leedle, H. Deng, J. S. Harris, R. L. Byer, and P. Hommelhoff, *Nucl. Instrum. Methods Phys. Res., Sect. A* **865**, 84 (2017).
- [24] D. Guénot, D. Gustas, A. Vernier, B. Beaufort, F. Böhle, M. Bocoum, M. Lozano, A. Jullien, R. Lopez-Martens, A. Lifschitz, and J. Faure, *Nat. Photonics* **11**, 293 (2017).
- [25] B.-H. Chen, E. Wittmann, Y. Morimoto, P. Baum, and E. Riedle, *Opt. Express* **27**, 21306 (2019).
- [26] F. O. Kirchner, A. Gliserin, F. Krausz, and P. Baum, *Nat. Photonics* **8**, 52 (2014).
- [27] G. M. Vanacore, I. Madan, G. Berruto, K. Wang, E. Pomarico, R. J. Lamb, D. McGrouther, I. Kaminer, B. Barwick, F. J. García de Abajo, and F. Carbone, *Nat. Commun.* **9**, 2694 (2018).
- [28] Y. Morimoto and P. Baum, *Phys. Rev. A* **97**, 033815 (2018).
- [29] J. Itatani, F. Quéré, G. L. Yudin, M. Y. Ivanov, F. Krausz, and P. B. Corkum, *Phys. Rev. Lett.* **88**, 173903 (2002).
- [30] M. Kitzler, N. Milosevic, A. Scrinzi, F. Krausz, and T. Brabec, *Phys. Rev. Lett.* **88**, 173904 (2002).
- [31] P. Eckle, M. Smolarski, P. Schlup, J. Biegert, A. Staudte, M. Schöffler, H. G. Müller, R. Dörner, and U. Keller, *Nat. Phys.* **4**, 565 (2008).
- [32] D. Ehberger, A. Ryabov, and P. Baum, *Phys. Rev. Lett.* **121**, 094801 (2018).
- [33] See Supplemental Material at <http://link.aps.org/supplemental/10.1103/PhysRevLett.125.193202> for details of experiment and analysis, which includes Refs. [34–40].
- [34] Y. Morimoto, Y. Shinohara, M. Tani, B.-H. Chen, K. L. Ishikawa, and P. Baum, [arXiv:1910.11821](https://arxiv.org/abs/1910.11821).
- [35] P. Baum and A. H. Zewail, *Proc. Natl. Acad. Sci. U.S.A.* **104**, 18409 (2007).
- [36] J. Koshobu and T. Iwata, *J. Spectrosc. Soc. Jpn.* **42**, 236 (1993).
- [37] D. Ehberger, C. Kealhofer, and P. Baum, *Struct. Dyn.* **5**, 044303 (2018).
- [38] P. Baum, *Chem. Phys.* **423**, 55 (2013).
- [39] R. Dahan, S. Nehemia, M. Shentcic, O. Reinhardt, Y. Adiv, X. Shi, O. Be'er, M. H. Lynch, Y. Kurman, K. Wang, and I. Kaminer, *Nat. Phys.*, <https://doi.org/10.1038/s41567-020-01042-w>.
- [40] O. Kfir, H. Lourenço-Martins, G. Storeck, M. Sivilis, T. R. Harvey, T. J. Kippenberg, A. Feist, and C. Ropers, *Nature (London)* **582**, 46 (2020).
- [41] L. Zhao, Z. Wang, H. Tang, R. Wang, Y. Cheng, C. Lu, T. Jiang, P. Zhu, L. Hu, W. Song, H. Wang, J. Qiu, R. Kostin, C. Jing, S. Antipov, P. Wang, J. Qi, Y. Cheng, D. Xiang, and J. Zhang, *Phys. Rev. Lett.* **122**, 144801 (2019).
- [42] D. Zhang, A. Fallahi, M. Hemmer, H. Ye, M. Fakhari, Y. Hua, H. Cankaya, A.-L. Calendron, L. E. Zapata, N. H. Matlis, and F. X. Kärtner, *Optica* **6**, 872 (2019).
- [43] L. Zhao, H. Tang, C. Lu, T. Jiang, P. Zhu, L. Hu, W. Song, H. Wang, J. Qiu, C. Jing, S. Antipov, D. Xiang, and J. Zhang, *Phys. Rev. Lett.* **124**, 054802 (2020).
- [44] E. C. Snively, M. A. K. Othman, M. Kozina, B. K. Ofori-Okai, S. P. Weathersby, S. Park, X. Shen, X. J. Wang, M. C. Hoffmann, R. K. Li, and E. A. Nanni, *Phys. Rev. Lett.* **124**, 054801 (2020).
- [45] P. Baum, *J. Appl. Phys.* **122**, 223105 (2017).
- [46] H. Vincenti and F. Quéré, *Phys. Rev. Lett.* **108**, 113904 (2012).
- [47] A. Feist, K. E. Echternkamp, J. Schauss, S. V. Yalunin, S. Schäfer, and C. Ropers, *Nature (London)* **521**, 200 (2015).
- [48] Y. Pan, B. Zhang, and A. Gover, *Phys. Rev. Lett.* **122**, 183204 (2019).
- [49] G. G. Paulus, F. Grasbon, H. Walther, P. Villoresi, M. Nisoli, S. Stagira, E. Priori, and S. De Silvestri, *Nature (London)* **414**, 182 (2001).
- [50] M. J. J. Kling, M. F. Siedschlag, Ch. Verhoef, A. J. Khan, J. I. Schultze, M. Uphues, Th. Ni, Y. Uiberacker, M. Drescher, M. Krausz, and F. Vrakking, *Science* **312**, 246 (2006).
- [51] M. Krüger, M. Schenk, and P. Hommelhoff, *Nature (London)* **475**, 78 (2011).
- [52] B. Piglosiewicz, S. Schmidt, D. J. Park, J. Vogelsang, P. Groß, C. Manzoni, P. Farinello, G. Cerullo, and C. Lienau, *Nat. Photonics* **8**, 37 (2014).
- [53] W. P. Putnam, R. G. Hobbs, P. D. Keathley, K. K. Berggren, and F. X. Kärtner, *Nat. Phys.* **13**, 335 (2017).
- [54] T. Rybka, M. Ludwig, M. F. Schmalz, V. Knittel, D. Brida, and A. Leitenstorfer, *Nat. Photonics* **10**, 667 (2016).
- [55] E. Curry, S. Fabbri, P. Musumeci, and A. Gover, *New J. Phys.* **18**, 113045 (2016).
- [56] M. Kozák, *Phys. Rev. Lett.* **123**, 203202 (2019).
- [57] A. Gover and A. Yariv, *Phys. Rev. Lett.* **124**, 064801 (2020).
- [58] Y. Pan and A. Gover, *Phys. Rev. A* **99**, 052107 (2019).